DOI: https://doi.org/10.2138/am-2021-7487. http://www.minsocam.org/

Revision 2

Age determination of oriented rutile inclusions in sapphire and of moonstone from the Mogok metamorphic belt, Myanmar

GUANGHAI SHI[1,*], XIAOCHONG ZHANG[1], YU WANG[1], QIULI LI[2**], FUYUAN WU[2], HUAIYU HE[2]

[1] State Key Laboratory of Geological Processes and Mineral Resources, China University of Geosciences, Beijing 100083, China, *E-mail: shigh@cugb.edu.cn

[2] State Key Laboratory of Lithospheric Evolution, Institute of Geology and Geophysics, Chinese Academy of Sciences, Beijing 100029, China, ** E-mail: liqiuli@mail.iggcas.ac.cn

ABSTRACT

The Mogok metamorphic belt (MMB), Myanmar, is one of the most well-known gemological belts on Earth. Previously, $^{40}Ar/^{39}Ar$, K-Ar, and U-Pb dating has yielded Jurassic - Miocene magmatic and metamorphic ages of the MMB and adjacent areas; however, no reported age data are closely related to the sapphire and moonstone deposits. Secondary ion mass spectrometry (SIMS) U-Pb dating of acicular rutile inclusions in sapphire and furnace step-heating $^{40}Ar/^{39}Ar$ dating of moonstone (antiperthite) in syenites from the MMB yield ages of 13.43 ± 0.92 and 13.55 ± 0.08 Ma, respectively, indicating both Myanmar sapphire and moonstone formed at the same time, and the ages are the youngest published in the region. The ages provide insight into the complex histories and processes of magmatism and metamorphism of the MMB, the formation of gemstone species in this belt, and the collision between India and Asia. In addition, our high field strength element data for the oriented rutile inclusions suggest an origin by coprecipitation, rather than exsolution. In-situ age determination of this nature is particularly significant, since rutile inclusions in other gemstones, such as rubies, can be used to help constrain geological history of their host rocks elsewhere.

Keywords: Rutile inclusion, moonstone, Mogok metamorphic belt, geochronology, syenite

INTRODUCTION

The Mogok metamorphic belt (MMB) is one of the most famous and important geological units. The MMB not only hosts many kinds of high quality gemstone but also forms a prominent tectonic sliver that is important for understanding the origin and continental evolution of Southeast Asia. Any list of historically most important gem deposits of the world must include the MMB, for its possession of the world's finest ruby and spinel, and for being the rich source of great varieties of gemstones, including sapphire, peridot, apatite, amblygonite, aquamarine, goshenite, scapolite, feldspar (moonstone, orthoclase, labradorite, microcline), pyroxene (diopside, enstatite, ferrosilite), hornblende (edenite, pargasite), andalusite, kyanite, fibrolite, zircon, garnet (almandine, grossular, hessonite, spessartite), alexandrite, chrysoberyl, iolite, quartz (amethyst, citrine), lapis-lazuli (lazurite), danburite, scheelite, titanite, topaz, tourmaline (rubellite, elbaite, schorl), hackmanite etc., as well as some rare sorts like painite, poudretteite, periclase, johachidolite, sodalite, taaffeite, ekanite, axinite, chondrodite, sinhalite, jeremejevite, kornerupine, etc. (e.g., Themelies 2008 and references therein; Harlow and Bender 2013; Guo et al. 2016; Wu et al. 2019). Gem mining in the MMB is thought to have started around 1044 AD (Themelies 2008). Mogok City is an active area for gem mining and trade, and the MMB continues attracting the attentions of mineral enthusiasts and researchers. The MMB potentially links the metamorphic and magmatic belts on the south margins of the Lhasa and Karakoram terranes, which face directly during the Indian collision. The MMB is thought to have accommodated the extrusion or rotation of Indochina away from the collision, along with major shear zones including the Ailao Shan-Red River shear belt in China, the Wang Chao and Three Pagodas faults in Thailand, and the Sagaing Fault in Myanmar (Lacassin et al. 1997); therefore, the magmatic, metamorphic and structural evolutions of the MMB place important constraints on the tectonic evolution of Southeast Asia (Barley et al. 2003). Previous geochronological studies have reported Cenozoic ages for rocks from the MMB (e.g., Mitchell 1993; Bertrand and Rangin 2003; Barley et al. 2003; Garnier et al. 2006; Mitchell et al. 2012; Lee et al. 2016; Win et al. 2016); however, the age data are dispersed (e.g., Bertrand and Rangin 2003), and no data have been reported for constraining the age of sapphire and moonstone in the MMB.

Sapphire is a gem variety of the corundum, and the chromophores in blue sapphire are Fe^{2+} and Ti^{4+}. Blue sapphires occur in dozens of localities on Earth, among which from Myanmar is thought to be one of the finest (Giuliani and Groat 2019 and references therein). There are two types of sapphire deposits, magmatic and metamorphic, and most magmatic sapphire are found in alkali basalts, lamprophyres and syenites (Guo et al. 1996; Sutherland et al. 1998, 2009; Harlow and Bender 2013; Giuliani and Groat 2019). Direct dating of corundum is impossible due to lack of a suitable geochronometer; therefore, ages are constrained by dating related minerals (e.g., zircon, monazite, rutile, and micas), either in the host rocks or as syngenetic inclusions in the corundum. One such example is rutile inclusions. They are observed frequently as needle in gem sapphire (Gübelin and Koivula 2004; Themelies 2008).

Rutile occurs as a characteristic mineral in moderate- to high- pressure metapelites, high pressure metamorphosed mafic rocks, and sedimentary rocks, and as an accessory mineral in plutonic igneous rocks (e.g., Mezger et al. 1989, 1991; Zack et al. 2002; Timmermann et al. 2004; Shi et al. 2012b; Li et al. 2013; Tropper 2014; Zack and Kooijman 2017), as well as occurring as either stubby inclusions (e.g., Wei et al. 2009; Sorokina et al. 2017), or as thin needles in corundum and other host minerals (Gübelin and Koivula 2004; Themelies 2008). In gem quality corundum, rutile occurs mostly as acicular inclusions known as “silk” in rubies and sapphires from Myanmar and Sri Lanka, where only silk rutile is reported, with no large grain rutile inclusions (Gübelin and Koivula 2004). Grain rutile inclusions in corundum have provided good opportunities for

This is the peer-reviewed, final accepted version for American Mineralogist, published by the Mineralogical Society of America.
The published version is subject to change. Cite as Authors (Year) Title. American Mineralogist, in press.
DOI: https://doi.org/10.2138/am-2021-7487. http://www.minsocam.org/

U-Pb dating (e.g., Sorokina et al. 2017); however, no such dating had been attempted on acicular rutile inclusions in minerals, including sapphire.

Moonstone (known as perthite and antiperthite in mineralogy) is composed of two feldspar species, orthoclase and albite, and shows an iridescent phenomenon called 'schiller'. Previous researches on moonstone focused mainly on its structure and exsolution mechanism (e.g., Tutton 1921; Tatekawa et al. 1972), no $^{40}Ar/^{39}Ar$ and K-Ar dating results have been reported.

We present U-Pb dating on acicular rutile included in sapphire, and $^{40}Ar/^{39}Ar$ age for moonstone in syenites from the MMB, and discuss their implications. The two ages are found to be similar and are the youngest published ages for rocks in the MMB.

GEOLOGICAL SETTING

Sapphire and moonstone-bearing syenites occur within the MMB, a narrow elongated sigmoidal belt (Fig. 1). The MMB is oriented approximately N-S, alongside the north- south trending Sagaing dextral strike-slip fault to the west and the Shan fault scarp to the east. It is more than 1000 km long and about 20-40 km wide (Mitchell et al. 2007; Searle et al. 2007), extending from the Gulf of Moittama (formerly Mantaban) in Lower Myanmar, through Mogok to Putao in Upper Myanmar, and can be traced northward to the Eastern Himalayan Syntaxis. The northwest part hosts the famous jadeite and Cretaceous amber mines (Shi et al. 2008, 2012a). The MMB consists of amphibolite-facies and locally granulite facies marbles, schists and gneisses intruded by variably deformed granitoids and pegmatites. Near Mogok, the high temperature, high pressure pyroxene- and sillimanite-bearing gneisses are interspersed with marbles. Based on the measurement of a garnet-biotite-plagioclase-sillimanite-quartz assemblage, the equilibrium pressure and temperature were suggested to be 0.6-1.0 GPa and 780–850 °C for the peak metamorphic stage, and 0.3-0.5 GPa and 600-680 °C for the exhumation and hydration stage (Win et al. 2016).

Several thermal events in the MMB had been reported. The oldest rock in the MMB was determined to be ca. 491 Ma for orthogneiss north of Mandalay, interpreted to be the age of its protolith (Mitchell et al. 2012 and references therein). The oldest undeformed intrusive rocks in the MMB is a ca.128 Ma diorite near Yebokson, while latter undeformed intrusions include a ca. 91 Ma diorite near Mokpalin, the weakly foliated ca. 72 Ma garnet-bearing granite near Nattaung, 44 and 48 Ma granites, and 20-17 Ma granite dykes (Mitchell et al. 2012). Emplacement ages of 35-23 Ma were reported for syntectonic hornblende syenites and leucogranites (Barley et al. 2003), and rubies from Mogok probably formed at 18.7-17.1 Ma (Garnier et al. 2006).

Mogok sapphires occur in/around the contact zone between alkali feldspar syenite pegmatite body and marble, or in the skarn. Differing from Mogok rubies, Mogok sapphires do not occur in marble. Their host rocks of the sapphire can be grouped into two types: nepheline syenite and alkali feldspar pegmatite. The presence of two-phase inclusions (aqueous fluids and gas bubble) in the sapphire indicates that metasomatism may have overlapped with the growth of the sapphires in magma (Themelis 2008). They

This is the peer-reviewed, final accepted version for American Mineralogist, published by the Mineralogical Society of America.
The published version is subject to change. Cite as Authors (Year) Title. American Mineralogist, in press.
DOI: https://doi.org/10.2138/am-2021-7487. http://www.minsocam.org/

are mined in the Pan-sho, Kyat-pyin, Kyauk-pyat-that, Baw-mar, Lay-thar, and On-dan areas. We obtained rutile-bearing sapphire sourced from the On-dan syenite mine (Fig. 1, 2), ~27 km NW from Mogok Township, from a local gemstone miner and dealer.

Moonstones in Mogok occur in syenite and pegmatite, and in alluvium (Themelis 2008 and reference therein). Two kinds of moonstone are present: Albite- and adularia-dominant moonstones. The two varieties are often indifferentiable by the near identical appearance. Albite-dominant moonstone occurs mainly in Sakhan-gyi, while adularia-dominant moonstone occurs in numerous localities. Most gem dealers agree that the MMB is the source of the best quality moonstone in the world. We obtained albite-dominant moonstone sourced from the Sakhan-gyi mine (Fig. 1, 3), ~15 km west of Mogok Township, from another local miner and dealer. The On-dan and Sakhan-gyi mines are located ~14 km apart.

METHODS

Rutile Raman and U-Pb analyses

The corundum sample was a polished round cabochon (2.20 cm in diameter, 0.6 cm in height) displaying hexagonal straight-edge color and growth zoning (Fig. 2). It is translucent, contained orientated rutile needle, and shows clear, bright asterism effects under oblique or perpendicular illumination. The corundum sample was set in a one inch diameter resin mount. It was ground with 3000 mesh disc, 2 minutes increments until suitable sized rutile needles appeared on the surface. Then it was polished to give a smooth, flat surface. Four rutile inclusions were exposed; however, only two of them, Rut-1 and -2, were large enough (~20 μm) for SIMS analyses.

The Raman spectra of the rutile inclusions were acquired using a HORIBA Jobin-Yvon LabRAM HR 800 at the Institute of Geology and Geophysics, Chinese Academy of Sciences, Beijing (IGGCAS), equipped with a Peltier cooled multichannel CCD detector and coupled with an Olympus BX41 petrographic microscope. A frequency-doubled Nd: YAG laser was used for excitation (λ = 532 nm, output power = 45 mW), with a grating of 600 lines/mm, a confocal hole of 400 μm, and a slit width of 100 μm. The monocrystalline silicon with a Raman shift at 520.7 cm^{-1} was used for calibration before measurement. The Raman spectra of the phases were acquired using a 100× objective with a 30 s acquisition time and three accumulations.

The procedure for rutile U-Pb isotopic analysis followed that of Li et al. (2011) and is summarized briefly here. The U-Pb isotopic analyses were performed using a CAMECA IMS 1280HR at IGGCAS. An O^{-} primary ion beam with an intensity of ~15 nA was used. The ellipsoidal spot was about 10 x 15 μm in size. The Pb/U ratios were calibrated using the DXK rutile standard (1782.6 ± 2.8 Ma; Li et al. 2013) and monitored using a JDX rutile standard (518 ± 4 Ma; Li et al. 2013). Common Pb was corrected for using the ^{207}Pb method.

Moonstone geochemical and dating analyses

Chemical compositions and backscattered electron images of the studied moonstone were acquired using an electron probe microanalyzer (Shimadzu Corporation EPMA-1720) at the Institute of Earth Sciences, China University of Geosciences, Beijing (CUGB). The operating conditions and standards used were the same as those described by Gao et al. (2019). The analytical precisions for the major and minor elements were ± 1.5% and ±10%, respectively. The $^{40}Ar/^{39}Ar$ dating on the moonstone was carried out using a Micromass MM-5400 spectrometry at CUGB. The J factor was estimated by repeated analyses of Fish Canyon Tuff sanidine, with an age of 27.55 ± 0.08 Ma and of the ZBH biotite, a Chinese standard with an age of 133.3 ± 0.24 Ma (Wang et al. 2011 and references therein), with 1% relative standard deviation (1σ).

RESULTS

Rutile

The Raman analyses showed peaks at 440 and 614 cm^{-1}, demonstrating the inclusions are rutile (Fig. 4). Two in-situ U-Pb analyses (Table 1) were performed on the two larger rutile inclusions, which yielded a lower intercept $^{238}U/^{206}Pb$ age of 13.43 ± 0.92 Ma on the Tera-Wasserburg plot (Fig. 5). After the rutile U-Pb analyses, we spent considerable time grinding and polishing the sapphire to find more suitable rutiles; however, we were unsuccessful and the dated rutiles were grinned away.

Moonstone

The EPMA data showed that the studied moonstone is an antiperthite with an albite matrix ($Ab_{90}An_8Or_2$) containing orthoclase-rich lamella ($Ab_{48}Or_{45}An_7$) (Table 2; Fig. 3). The $^{40}Ar/^{39}Ar$ analysis produced a weighted mean plateau age of 13.55 ± 0.08 Ma. An inverse isochron age of 13.71 ± 0.59 Ma (MSWD = 0.82), calculated from eight steps that form the plateau, is consistent with the plateau age (Table 3; Fig. 6). This age is almost the same as the rutile U-Pb age of 13.43 ± 0.92 Ma.

DISCUSSION

Rutile petrogenesis

Under the microscope, oriented rutile needles were seen in two forms, most of which were fine needles of 10-20 μm long and ~1.0 μm wide and aligned perpendicular to the c-axis. The rutile needles are parallel to the crystallographic directions, intersecting at an angle of 60°/120° (Fig. 2). Coarser rutile needles up to ~20 um wide could be seen occasionally and heterogeneously, but oriented. By scrutinizing under the gemological microscope, no protogenetic or randomly oriented rutile grain was found. The images of Rt-1 and Rt-2 (Fig. 2) show sharp edges with big aspect ratio and unambiguous tetragonal outlines, without double tetragonal symmetry pyramid outline on both ends. In contrast, section images of random rutile grain inclusions in corundum from other localities are much larger in size, and obviously rounded, with double tetragonal symmetry pyramid outline on both ends (e.g., Wei et al. 2009; Sorokina et al. 2017). The inclusion characteristics are similar to those of typical Myanmar sapphire described by Gübelin and

DOI: https://doi.org/10.2138/am-2021-7487. http://www.minsocam.org/

Koivula (2004), who reported that the fine rutile needles unite to form broad zones, while coarser rutile needles form "silk" texture. The "silk" rarely consists of rutile fibers, but instead consists of brown rutile grains arranged in straight rows. There are dolomite, pyrrhotite, and small, unexpected protogenetic brookite inclusions in the sapphire reported by Gübelin and Koivula (2004); however, they did not find any randomly arranged rutile inclusions.

Our high field strength element data for the oriented rutile inclusions suggest they formed by coprecipitation, rather than by exsolution. The contents of U (24-149 ppm) and Th (3.09-4.57 ppm) in rutile needles are even higher than in metamorphic rutile grains from Daixian (U = 9.0-28.3 ppm, mean=17.8, Th = 0.126 ppm) reported by Shi et al. (2012b). The U and Th have ionic radii of 0.97-1.01 and 1.02-1.06 Å, respectively, much larger than that of Ta, W, Nb and Zr (Palke and Breeding 2017). The U^{4+} and Th^{4+} should be more difficult to be incorporated into corundum than Nb^{5+}, Ta^{5+}, and W^{6+}, owing to the mismatches in their ionic radii and the large differences in their ionic charge compared to Al^{3+} (Palke and Breeding, 2017); after all, such high field strength elements are readily incorporated into rutile (Zack et al. 2002). The high U and Th contents substituting Ti in the oriented rutile inclusions are more consistent with the rutile inclusion forming by coprecipitation than exsolution. It is worth noting that there are no melt inclusions in Myanmar sapphire, unlike that reported by Palke and Breeding (2017); therefore, we cautiously use the term "mineral exsolution" when referring to the aligned rutile inclusions in sapphires.

Age interpretations

A reasonable estimation of the closure temperature (Tc) for rutile U-Pb systems is a key factor in the interpretation of the ages. Although Tc of rutile U-Pb system was debated (Mezger et al. 1989; Cherniak 2000; Li et al. 2003, 2011; Vry and Baker 2006), the recent consensus is that this temperature is strongly dependent on grain size, ranging from > 600 °C at the core of large grains to ~490 ºC near the rim (see Kooijman et al. 2010). Although the studied rutile is ~20 μm wide, it is hosted within rigid gem-quality corundum, a reasonable estimation of Tc would be 500-600 °C.

Field evidence, petrographic observations and geochemical data suggest that the sapphire-bearing alkali-feldspar syenite pegmatite was derived mainly by magmatic differentiation (Thu 2007). Abundant volatiles are evidenced by the large crystals and a wide variety of rare accessory minerals, and the pegmatitic texture of the syenite. Volatiles are thought to introduce alumina into corundum in the dyke. The liquidus temperature of the augite-biotite granite was estimated to be ~700 ºC (Thu 2007), and the syenite dyke formed at a temperature no higher than that of granite; therefore, the $^{238}U/^{206}Pb$ age of 13.43 ± 0.92 Ma is likely the formation age of the hosted sapphire, or slightly younger, as well as of the hosted syenite. Theoretically, the closure temperature for the $^{40}Ar/^{39}Ar$ system in K-feldspar ranges from 200 to 350 °C (Dodson 1973; McDougall and Harrison 1999; Van der Pluijm and Marshak 2004; Wang et al. 2020). Given the form of host rock, the cooling rate of the moonstone is likely to be >50 °C/My, and a closure temperature of ~300 °C is a good estimate. Consequently, the weighted mean plateau age of 13.55 ± 0.08 Ma for the moonstone records the last time when the moonstone reached a temperature of ~300 °C.

Given the almost identical ages and the difference >200 ºC between the Tc for the rutile U-Pb and moonstone $^{40}Ar/^{39}Ar$ systems, the age of ca. 13.5 Ma is interpreted as either the formation time of the two minerals or the total reset age; however, an age of ca. 13.5 Ma has not been reported previously. This age is unlike to represent a regional thermal event, which would have led to other rocks recording ages of ca. 13.5 Ma; Therefore, our preferred interpretation is that the sapphire and moonstone formed at ca. 13.5 Ma.

The age of ca. 13.5 Ma is the youngest among all published ages in the MMB, including published $^{40}Ar/^{39}Ar$ ages (Table 4; e.g., Garnier et al. 2006; Mitchell et al. 2012). **T**he MMB consists of a series of undifferentiated high-grade metasedimentary and meta igneous rocks; the common lithologies include gneiss, schist, quartzite, marble, calcsilicate rock and migmatite, with various granitoid intrusions (Barley et al. 2003; Mitchell et al. 2007; Searle et al. 2007, 2020; Thu et al. 2016, 2017). Many radiometric ages have been reported for the metamorphic and tectonic evolution of the Mogok belt and adjacent areas (Table 4). Bertrand et al. (1999, 2001) reported Oligocene-Middle Miocene $^{40}Ar/^{39}Ar$ and K-Ar ages for biotite and muscovite. Granit SHRIMP U-Pb zircon ages indicate that magmatism occurred during the Jurassic and a later high-grade metamorphic recrystallization event took place during the Eocene (Barley et al. 2003).

Searle et al. (2007, 2020) reported U-Th-Pb ages of metamorphic monazite, zircon, xenotime and thorite and suggested two distinct metamorphic events: a Paleocene event, which implies earlier regional metamorphism (ca. 59 Ma); and a Late Eocene to Oligocene event (ca. 24.5 Ma), which was interpreted as the peak in metamorphism that resulted in syn-metamorphic crustal melting, producing garnet and tourmaline-bearing leucogranite. Win et al. (2016) reported that the peak upper amphibolite or granulite facies metamorphism was late Eocene in age, and the subsequent hydration stage was as late Oligocene on the basis of dates from metamorphic monazite. The youngest reported magmatic event happened in late Oligocene-early Miocene, producing mantle-derived syntectonic hornblende syenite and crust-derived leucogranite, postdating the high temperature metamorphism and intrusion (Bertrand et al. 1999; Barley et al. 2003; Searle et al. 2007). Garnier et al. (2006) reported $^{40}Ar/^{39}Ar$ ages of 18.7-17.1 Ma for phlogopite in ruby-bearing marble near Mogok, which is 4 My older than our samples. The Kabaing microgranite yielded a magmatic U-Pb zircon age of 16.8 ± 0.5 Ma (Gardiner et al. 2016, 2018), almost the same as the 16 Ma age reported by Searle and Haq (1964), and the biotite $^{40}Ar/^{39}Ar$ age of 15.8 ± 1.1 Ma reported by Bertrand et al. (2001). Another similarly young age is the 16.1 ± 0.5 Ma, U-Th-Pb dating of zircon age for painite-bearing skarn at the contact between the Pingutaung leucogranite and marble (Thu 2007). Our youngest age provides new evidence for understanding this complex, which may have implications for our understanding of the formation of the Mogok gemstone belt, as well as the collision between India and Asia.

IMPLICATIONS

Our youngest age confirms that the MMB experienced several more thermal events or other geodynamic processes than previously believed, and we propose that the gemstone formations in this deposit suggest two or more thermal events.

Our young age also shows that the MMB is connected with and responded to the collision between India and Asia which formed the Tibetan Plateau and Himalayan orogen (Harrison et al. 1992). The Burma terrane collided with Asia during the Late Jurassic-Early Cretaceous, becoming the neighboring Lhasa terrane that occupies the southern part of the Tibetan Plateau (Mitchell 1993; Licht et al. 2013). The MMB formed by the partial exhumation of the deep basement of the Burma terrane, and is the transition region between the Central Myanmar Basin and the Shan–Thai block (Bertrand and Rangin 2003; Mitchell et al. 2007, 2012). Numerous Cenozoic ages, from 55-50 Ma, to as young as 8 Ma, are reported for igneous rocks in the Lhasa terrane (e.g., Hou et al. 2004, 2009; Zhao et al. 2009; Xu et al. 2017), and ultrapotassic rocks, porphyries and adakitic intrusions have the ages of ca. 13.5 Ma.

This study could be a pioneer investigation to show that the oriented rutile needles (though with coarse ones) in sapphires could serve as a geochronometer to record meaningful geological events. This procedure could be valuable for dating other sapphire crystals with aligned rutile needles, such as those from Sri Lanka (Gübelin and Koivula 2004), Shandong, China (He et al. 2011) and possibly other localities (e.g., Sutherland et al. 2009; Sorokina et al. 2015). In addition, it is also possible to date other minerals containing rutile inclusions besides corundum crystals, including quartz, diamond, and garnet. Further geochronological data would play an increasingly import role in geosciences, especially the exploration of gem generation and ore prospecting.

ACKNOWLEDGEMENTS

We appreciate Prof. R.X. Zhu and T.T. Nyunt for their kind supports during the field trip in Myanmar, J.W. Yin and P.X. Lai for their help with EMP analyses, and X.X. Ling, Y. Liu, T. Zhou, H.X. Ma for SIMS and Raman analyses. Constructive comments and suggestions by Prof. F.Z. Teng and two anonymous referees are gratefully acknowledged.

FUNDING

This work was supported by the National Science Foundation of China (41688103, 41773044).

REFERENCES

Barley, M.E., Pickard, A.L., Zaw, K., Rak, P., and Doyle, M.G. (2003) Jurassic to Miocene magmatism and metamorphism in the Mogok metamorphic belt and the India-Eurasia collision in Myanmar. Tectonics, 22(3), 1-11.

Bertrand, G., and Rangin, C. (2003) Tectonics of the western margin of the Shan plateau (central Myanmar): implication for the India–Indochina oblique convergence since the Oligocene. Journal of Asian Earth Sciences, 21(10), 1139-1157.

Bertrand, G., Rangin, C., Maluski, H., Han, T.A., Thein, M., Myint, O., Maw, W., and Lwin, S. (1999) Cenozoic metamorphism along the Shan Scarp (Myanmar): Evidences for ductile shear along the Sagaing Fault or the northward migration of the Eastern Himalayan Syntaxis? Geophysical Research Letters, 26(7), 915-918.

Bertrand, G., Rangin, C., Maluski, H., and Bellon, H. (2001) Diachronous cooling along the Mogok Metamorphic Belt (Shan scarp, Myanmar): the trace of the northward migration of the Indian syntaxis. Journal of Asian Earth Sciences, 19(5), 649-659.

Cherniak, D.J. (2000) Pb diffusion in rutile. Contributions to Mineralogy and Petrology, 139(2), 198-207.

Dodson, M.H. (1973) Closure temperature in cooling geochronological and petrological systems. Contributions to Mineralogy and Petrology, 40(3), 259–274.

Gao, K., Shi, G.H., Wang, M.L., Xie, G., Wang, J., Zhang, X.C., Fang, T., Lei, W.Y., and Liu, Y. (2019) The Tashisayi nephrite deposit from South Altyn Tagh, Xinjiang, northwest China. Geoscience Frontiers, 10(4), 1597-1612.

Gardiner, N.J., Robb, L.J., Morley, C.K., Searle, M.P., Cawood, P.A., Whitehouse, M.J., Kirkland, C.L., Roberts, N.M.W., and Myint, T.A. (2016) The tectonic and metallogenic framework of Myanmar: A Tethyan mineral system. Ore Geology Reviews, 79, 26-45.

Garnier, V., Maluski, H., Giuliani, G., Ohnenstetter, D., and Schwarz, D. (2006) Ar-Ar and U-Pb ages of marble-hosted ruby deposits from central and southeast Asia. Canadian Journal of Earth Sciences, 43(4), 509-532.

Gardiner, N.J., Searle, M.P., Morley, C.K., Robb, L.J., Whitehouse, M.J., Roberts, N.M.W., Kirkland, C.L., and Spencer, C.J. (2018) The crustal architecture of Myanmar imaged through zircon U-Pb, Lu-Hf and O isotopes: Tectonic and metallogenic implications. Gondwana Research, 62, 27-60.

Giuliani, G., and Groat, l.A. (2019) Geology of corundum and emerald gem deposits: a review. Gems & Gemology, 55(4), 464–489.

Gübelin, E.J., and Koivula, J.I. (2004) Photoatlas of inclusions in Gemstones (4th edition). Opinio Verlag Basel, Switzerland.

Guo, J.F., Oreilly, S.Y., and Griffin, W.L. (1996) Corundum from basaltic terrains: A mineral inclusion approach to the enigma. Contributions to Mineralogy and Petrology, 122(4), 368-386.

Guo, S., Chen, Y., Liu, C.Z., Wang, J.G., Su, B., Gao, Y.J., Wu, F.Y., Sein, K., Yang, Y.H. and Mao, Q. (2016) Scheelite and coexisting F-rich zoned garnet, vesuvianite, fluorite, and apatite in calc-silicate rocks from the Mogok metamorphic belt, Myanmar: Implications for metasomatism in marble and the role of halogens in W mobilization and mineralization. Journal of Asian Earth Sciences, 117, 82–106.

Harlow, G.E., and Bender, W. (2013) A study of ruby (corundum) compositions from the Mogok Belt, Myanmar: Searching for chemical fingerprints. American Mineralogist, 98(7), 1120–1132

Harrison, T.M., Copeland, P., Kidd, W.S.F., and Yin, A., (1992) Raising Tibet. Science, 255, 1663–1670.

He, H., Zhu, R., and Saxton, J. (2011) Noble gas isotopes in corundum and peridotite xenoliths from the eastern North China Craton: Implication for comprehensive refertilization of lithospheric mantle. Physics of the Earth and Planetary Interiors, 189(3-4), 185-191.

Hou, Z.Q., Gao, Y.F., Qu, X.M., Rui, Z.Y., and Mo, X.X. (2004) Origin of adakitic intrusives generated during mid-Miocene east–west extension in southern Tibet. Earth and Planetary Science Letters, 220, 139–155.

Hou, Z.Q., Yang, Z.M., Qu, X.M., Meng, X.J., Li, Z.Q, Beaudoin, G. Rui, Z.Y, Gao, Y,F., and Zaw K. (2009) The Miocene Gangdese porphyry copper belt generated during post-collisional extension in the Tibetan Orogen. Ore Geology Reviews, 36, 25 – 51.

Kooijman, E., Mezger, K., and Berndt, J. (2010) Constraints on the U-Pb systematics of metamorphic rutile from in situ LA-ICP-MS analysis. Earth and Planetary Science Letters, 293(3-4), 321-330.

Lacassin, R., Maluski, H., Leloup, P.H., Tapponnier, P., Hinthong, C., Siribhakdi, K., Chuaviroj, S., and Charoenravat, A. (1997) Tertiary diachronic extrusion and deformation of western Indochina: Structural and $^{40}Ar/^{39}Ar$ evidence from NW Thailand. Journal of Geophysical Research-Solid Earth, 102(B5), 10013-10037.

Lee, H., Chung, S., and Yang, H. (2016) Late Cenozoic volcanism in central Myanmar: Geochemical characteristics and geodynamic significance. Lithos, 245, 174-190.

Li, Q.L., Li, S.G., Zheng, Y.F., Li, H.M., Massonne, H.J., and Wang, Q.C. (2003) A high precision U-Pb age of metamorphic rutile in coesite-bearing eclogite from the Dabie Mountains in central China: a new constraint on the cooling history. Chemical Geology, 200(3-4), 255-265.

Li, Q.L, Lin, W., Su, W., Li, X., Shi, Y., Liu, Y., and Tang, G. (2011) SIMS U-Pb rutile age of low-temperature eclogites from southwestern Chinese Tianshan, NW China. Lithos, 122(1-2), 76-86.

Li, Q.L., Yang, Y.N., Shi, Y.H., and Lin, W. (2013) Eclogite rutile U-Pb dating: Constraint for formation and evolution of continental collisional orogen. Chinese Science Bulletin, 58(23), 2279-2284 (in Chinese).

Licht, A., France-Lanord, C., Reisberg, L., Fontaine, C., Aung Naing Soe, and Jaeger, J.J. (2013) A Paleo Tibet–Myanmar connection? Reconstructing the Late Eocene drainage system of central Myanmar using a multi-proxy approach. Journal of the Geological Society, 170, 929–939.

McDougall, I., and Harrison, T. M. (1999) Geochronology and thermochronology by the $^{40}Ar/^{39}Ar$ method, 269 p. Oxford University Press, New York.

Mezger, K., Hanson, G.N., and Bohlen, S.R. (1989) High-precision U-Pb ages of metamorphic rutile: Application to the cooling history of high-grade terranes. Earth and Planetary Science Letters, 96(1-2), 106-118.

Mezger, K., Rawnsley, C.M., Bohlen, S.R., and Hanson, G.N. (1991) U-Pb garnet, sphene, monazite, and rutile ages: Implications for the duration of high-grade metamorphism and cooling histories, Adirondack MTS, New-York. Journal of Geology, 99(3), 415-428.

Mitchell, A. (1993) Cretaceous-Cenozoic tectonic events in the western Myanmar (Burma) Assam region. Journal of the Geological Society, 150(6), 1089-1102.

Mitchell, A.H.G., Htay, M.T., Htun, K.M., Win, M.N., Oo, T., and Hlaing, T. (2007) Rock relationships in the Mogok metamorphic belt, Tatkon to Mandalay, central Myanmar. Journal of Asian Earth Sciences, 29(5-6), 891-910.

Mitchell, A., Chung, S., Oo, T., Lin, T., and Hung, C. (2012) Zircon U–Pb ages in Myanmar: Magmatic–metamorphic events and the closure of a neo-Tethys ocean? Journal of Asian Earth Sciences, 56, 1-23.

Palke, A.C., and Breeding, C.M. (2017) The origin of needle-like rutile inclusions in natural gem corundum: A combined EPMA, LA-ICP-MS, and nanoSIMS investigation. American Mineralogist, 102(7), 1451-1461.

Searle, D.L. and Haq, B.T. (1964) The Mogok belt of Burma and its relationship to the Himalayan orogeny. In G. Kohli, V.S. Krishnaswamy, and K.S. Valdiya, Eds., Report of the 22nd Session, India 1964, Part XI, Proceedings of Section 11: Himalayan and Alpine Orogeny, p. 132–161. International Geological Congress, New Delhi

Searle, M.P., Noble, S.R., Cottle, J.M., Waters, D.J., Mitchell, A.H.G., Hlaing, T., and Horstwood, M.S.A. (2007) Tectonic evolution of the Mogok metamorphic belt, Burma (Myanmar) constrained by U-Th-Pb dating of metamorphic and magmatic rocks. Tectonics, 26(3). TC3014.

Searle, M.P., Garber, J.M., Hacker, B.R., Htun, K., Gardiner, N.J., Waters, D.J., and Robb, L.J. (2020) Timing of syenite-charnockite magmatism and ruby and sapphire metamorphism in the Mogok valley region, Myanmar. Tectonics, 39(3) e2019TC005998.

Shi, G.H., Cui, W.Y., Cao, S.M., Jiang, N., Jian, P., Liu, D.Y., Miao, L.C., and Chu, B.B. (2008) Ion microprobe zircon U-Pb age and geochemistry of the Myanmar jadeitite. Journal of Geological Society, 165, 221-234.

Shi, G.H., Grimaldi, D.A., Harlow, G.E., Wang, J., Wang, J., Yang, M.C., Lei, W.Y., Li, Q.L., and Li, X.H. (2012a) Age constraint on the Burmese amber based on U-Pb dating of zircons. Cretaceous Research, 37, 155-163.

Shi, G.H., Li, X.H., Li, Q.L., Chen, Z.Y., Deng, J., Liu, Y., Kang, Z., Pang, E.C, Xu, Y.J., and Jia, X.M. (2012b) Ion microprobe U-Pb age and Zr-in-rutile thermometry of rutiles from the Daixian rutile deposit in the Hengshan Mountains, Shanxi Province, China. Economic Geology, 107(3), 525-535.

Sorokina, E.S., Litvinenko, A.K., Hofmeister, W., Haeger, T., Jacob, D.E., and Nasriddinov, Z.Z. (2015) Rubies and sapphires from Snezhnoe, Tajikistan. Gems & Gemology, 51(2), 160-175.

Sorokina, E.S., Rösel, D., Häger, T., Mertz-Kraus, R., and Saul, J.M. (2017) LA-ICP-MS U–Pb dating of rutile inclusions within corundum (ruby and sapphire): new constraints on the formation of corundum deposits along the Mozambique belt. Mineralium Deposita, 52(5), 641-649.

Sutherland, F.L., Hoskin, P., Fanning, C.M., and Coenraads, R.R. (1998) Models of corundum origin from alkali basaltic terrains: a reappraisal. Contributions to Mineralogy and Petrology, 133(4), 356-372.

Sutherland, F.L., Giuliani, G., Fallick, A.E., Garland, M., and Webb, G. (2009) Sapphire-ruby characteristics, west Pailin, Cambodia: Clues to their origin based on trace element and O isotope analysis. Australian Gemmologist, 23, 329–368.

Tatekawa, M., Kanezaki, M., and Nakano, S. (1972) On the perthite structure of moonstone (II) high temperature form of moonstone. Mineralogical Journal, 7(1), 9-28.

Themelis, T. (2008) Gems & mines of Mogok, 352 p. Ted Themelis, Thailand.

Thu, K. (2007) The igneous rocks of the Mogok stone tract: Their distributions, petrography, petrochemistry, sequence, geochronology and economic geology, 139 p. Ph.D. thesis, Yangon University, Yangon, Myanmar.

Thu, Y.K., Win, M.M., Enami, M., and Tsuboi, M. (2016) Ti-rich biotite in spinel and quartz-bearing paragneiss and related rocks from the Mogok metamorphic belt, central Myanmar. Journal of Mineralogical and Petrological Sciences, 111(4), 270-282.

Thu, Y.K., Enami, M., Kato, T., and Tsuboi, M. (2017) Granulite facies paragneisses from the middle segment of the Mogok metamorphic belt, central Myanmar. Journal of Mineralogical and Petrological Sciences, 112(1), 1-19.

Timmermann, H., Štědrá, V., Gerdes, A., Noble, S.R., Parrish, R.R., and Dörr, W. (2004) The problem of dating high-pressure metamorphism: A U-Pb isotope and geochemical study on eclogites and related rocks of the Marianske Lazne Complex, Czech Republic. Journal of Petrology, 45(7), 1311-1338.

Tropper, P. (2014) Small grains and big implications: Accessory Ti- and Zr-minerals as petrogenetic indicators in HP and UHP marbles. American Mineralogist, 99(7), 1197-1198.

Tutton, A.E.H. (1921) The structure of adularia and moonstone. Nature, 108(2715), 352-353.

Van der Pluijm, B.A., and Marshak, S. (2004) Earth structure (second edition), 656 p. Norton Publication House, New York.

Vry, J.K., and Baker, J.A. (2006) LA-MC-ICPMS Pb-Pb dating of rutile from slowly cooled granulites: Confirmation of the high closure temperature for Pb diffusion in rutile. Geochimica et Cosmochimica Acta, 70(7), 1807-1820.

Wang, Y., Zhou, L., and Li, J. (2011) Intracontinental superimposed tectonics: A case study in the Western Hills of Beijing, eastern China. Geological Society of America Bulletin, 123(5-6), 1033-1055.

Wang, Y., Zhou, L.Y., Horst, Z., Lo, C.H., Li, G.W., and Hao, J.H. (2020) $^{40}Ar/^{39}Ar$ dating of cataclastic K-feldspar: A new approach for establishing the chronology of brittle deformation. Journal of Structural Geology, 131, 103948.

Wei, R., Li, Y., Xie, Y., Shi, G.H., and Zhang, W.H. (2009) Characteristics of inclusions in lead-glass-filled ruby. Journal of Gems and Gemmology, 11(3), 22-25 (in Chinese).

Whitney, D.L. and Evans, B.W. (2010) Abbreviations for names of rock-forming minerals. American Mineralogist, 95, 185–187.

Win, M.M., Enami, M., and Kato, T. (2016) Metamorphic conditions and CHIME monazite ages of Late Eocene to Late Oligocene high-temperature Mogok metamorphic rocks in central Myanmar. Journal of Asian Earth Sciences, 117, 304-316.

Wu, L., Shi, G.H., Danisik, M., Wang, Y.Z., and Wang, F. (2019) MK-1 apatite: A new potential reference material for (U-Th)/He dating. Geostandards and Geoanalytical Research, 43(2), 301-315.

Xu, B., Griffin, W.L., Xiong, Q., Hou, Z.Q., O'Reilly, S.Y., Guo, Z., Pearson, N.J., Gréau, Y., Yang, Z.M., and Zheng, Y.C. (2017) Ultrapotassic rocks and xenoliths from South

Tibet: Contrasting styles of interaction between lithospheric mantle and asthenosphere during continental collision. Geology, 2017, 45(1), 51–54.

Zack, T., Kronz, A., Foley, S.F., and Rivers, T. (2002) Trace element abundances in rutile from eclogites and associated garnet mica schists. Chemical Geology, 184(1-2), 97-122.

Zack, T., and Kooijman, E. (2017) Petrology and geochronology of rutile. Reviews in Mineralogy and Geochemistry, 83(1), 443-467.

Zhao, Z., Mo, X., Dilek, Y., Niu, Y., DePaolo, D.J., Robinson, P., Zhu, D., Sun, C., Dong, G., and Zhou, S. (2009) Geochemical and Sr-Nd-Pb-O isotopic compositions of the post-collisional ultrapotassic magmatism in SW Tibet: Petrogenesis and implications for India intra-continental subduction beneath southern Tibet: Lithos, 113, 190–212.

Figure captions

FIGURE 1. (a) Simplified tectonic map of the Mogok metamorphic belt (after Mitchell et al. 2007 and Searle et al. 2007). Geological maps of the (b) On-dan and (c) Sakhan-gyi mines (Modified after Themelis 2008).

FIGURE 2. (a) Sapphire sample mounted in resin. (b) Photomicrograph of aligned acicular rutile inclusions in the corundum. (c, d) Photomicrographs under reflected light of the two polished rutile inclusions prepared for SIMS U-Pb dating. Mineral abbreviation after Whitney and Evans (2010).

FIGURE 3. a) Photograph of the moonstone sample and (b) Backscattered electron image of K-feldspar (Kf) lamellar within plagioclase (Pl).

FIGURE 4. Raman spectra of rutile needles in the corundum, showing that two rutile inclusions are large enough for Raman measurement, whereas the other two are too small.

FIGURE 5. U-Pb age of rutile inclusions in the sapphire on the Tera-Wasserburg Plot.

FIGURE 6. Age spectra and inverse isochron diagram of the moonstone sample.

TABLE 1. In-situ SIMS U-Pb results for rutile inclusions in the sapphire sample

No.	**U ppm**	**Th ppm**	**Th/U**	**Tera-Wasserburg Plot (total Pb)**				**f_{206}%**	**^{207}Pb-correction**	
				^{238}U/ ^{206}Pb	Error (%)	^{207}Pb/ ^{206}Pb	Error (%)		Age (Ma)	**Error (Ma)**
1	149	3.1	0.02	432.5	3.4	0.124	3.0	9.2	13.4	**0.5**
2	24	4.6	0.19	34.4	12	0.775	3.3	90.2	15.4	**7.9**

TABLE 2. Representative chemical compositions of the moonstone sample

point	Na_2O	MgO	Al_2O_3	SiO_2	CaO	P_2O_5	K_2O	FeO	MnO	TiO_2	Cr_2O_3	total	formula
Host	10.38	0	20.71	66.21	1.55	0.01	0.40	0.00	0	0.04	0.01	99.31	$Ab_{90}An_8Or_2$
Lamella	5.73	0.01	20.90	64.53	1.26	0.00	8.11	0.06	0.04	0.00	0.01	100.64	$Ab_{48}An_7Or_{45}$

TABLE 3. $^{40}Ar/^{39}Ar$ step heating data for the moonstone sample

T(℃)	$(^{40}Ar/^{39}Ar)_m$	$(^{36}Ar/^{39}Ar)_m$	$(^{37}Ar/^{39}Ar)_m$	$(^{40}Ar_R/^{39}Ar_k)_m$	$^{39}Ar(\times10^{-8}ccSTP)$	$^{39}Ar(\%)$	$^{40}Ar_R/^{40}Ar_T(\%)$	Age (Ma)	Error (Ma)
810	3438	10.84	242	311.5	0.000	0.00	8.51	656	8340
950	17135	57.62	182	142.7	0.000	0.00	2.01	330	51124
1060	1540	5.024	110	69.13	0.001	0.02	5.34	167	1012
1120	367.9	0.128	5.99	332.2	0.005	0.07	89.98	692	35
1160	249.3	0.829	4.01	4.697	0.039	0.54	3.16	11.90	7.81
1200	7.952	0.009	0.757	5.456	0.168	2.31	68.98	13.82	0.88
1240	7.090	0.005	0.498	5.588	0.155	2.13	79.06	14.15	0.90
1270	6.760	0.003	0.431	5.973	0.177	2.43	88.47	15.12	1.04
1300	6.875	0.003	0.650	5.940	0.209	2.87	86.54	15.04	0.66
1330	6.821	0.005	1.18	5.511	0.280	3.85	80.98	13.95	1.00
1360	6.506	0.003	0.315	5.783	0.377	5.17	89.01	14.64	0.59
1380	6.270	0.004	0.530	5.229	0.496	6.81	83.57	13.24	0.48
1390	6.001	0.002	0.000	5.332	1.007	13.8	89.00	13.50	0.13
1400	5.896	0.002	0.000	5.370	1.500	20.6	91.20	13.60	0.14
1410	5.876	0.002	0.000	5.288	2.869	39.4	90.12	13.39	0.13

W= 0.0348g J= 0.001409

TABLE 4. Summary of published ages (Ma) from the MMB

Description	Locality or near	U-Pb age (2σ)	$^{40}Ar/^{39}Ar$ age (2σ)	References
Ms granite	Payangazu	218.9 ± 2.5		Gardiner et al. 2018
granodiorite	Mandalay hills	171.7 ± 2.1		Barley et al. 2003
charnockite-syenite	Taung - met	170 - 168		Searle et al. 2020
Ms granite	Payangazu	123.4 ± 2.0		Gardiner et al. 2018
granodiorite	Yebokson	120.9 ± 0.9		Barley et al. 2003
Ms granite	Payangazu	71.9 ± 1.1		Gardiner et al. 2018
Bt granite	Nattanng	71.1 ± 0.6		Gardiner et al. 2018
granite	Belin quarry	59.5 ± 0.9		Searle et al. 2007
Bt-Kf granite	Byinge	55.1 ± 0.5		Gardiner et al. 2018
syenite	Mandalay Hill	47.25 ± 1.28		Barley et al. 2003
leucogranite	Kyaukse	45.5 ± 0.6		Searle et al. 2007
K-feldspar augen gneiss	Kyanigan	37.4 ± 1.3		Searle et al. 2007
syenite	Le Oo	37.2 ± 0.3		Searle et al. 2020
syenite	Mandalay Hill	33.11 ± 0.93		Barley et al. 2003
leucogranite	Pingutaung	32 ± 1		Thu 2007
syenite	Mandalay Hill	30.9 ± 0.7		Barley et al. 2003
sillimanite gneiss	Kyaukse north	29.3 ± 0.5		Searle et al. 2007
leucogranite	Kyanigan	24.5 ± 0.7		Searle et al. 2007
syenogranites	Yesin dam	22.6 ± 0.4		Barley et al. 2003
titanite, skarn	Le Oo	21.6 ± 0.6		Searle et al. 2020
tit**anite, skarn**	Le Oo	21.5 ± 0.6		Searle et al. 2020
apatite	Ohn-Gaing	18.0± 0.2		Wu et al. 2019
granite	Kabaing	16.8 ± 0.5		Gardiner et al. 2016
biotite	Thaton Area		25.9±0.8	Bertrand et al. 2001
biotite	Mandalay area		22.7±0.4	Bertrand et al. 2001
biotite	Mong-Iong		19.5 ±1.0	Bertrand et al. 2001
phlogopite	Mogok		18.7 ± 0.2	Garnier et al. 2006
biotite	Pyant-gyi		17.4 ± 0.6	Bertrand et al. 2001
phlogopite	Mogok		17.1 ± 0.2	Garnier et al. 2006
biotite	Mogok		16.5 ±0.6	Bertrand et al. 2001
biotite	Gwe-bin		15.8 ±1.1	Bertrand et al. 2001

Ms: mouscovite, Bt: biotite, Kf: K-feldspar

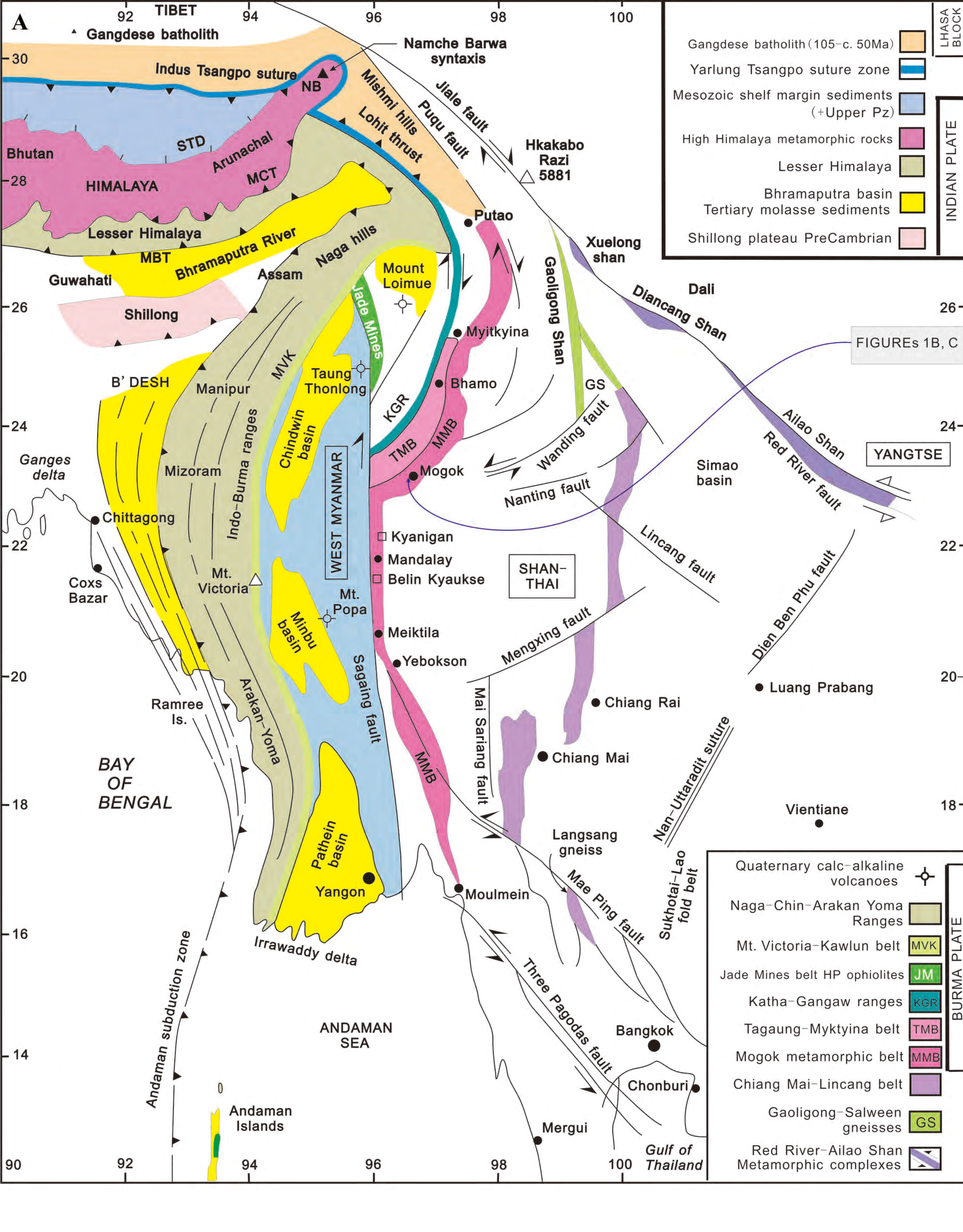
A
TIBET
Gangdese batholith
Namche Barwa syntaxis
Indus Tsangpo suture
NB
Mishmi hills
Lohit thrust
Puqu fault
Jiale fault
Hkakabo Razi 5881
Bhutan
STD
Arunachal
HIMALAYA
MCT
Lesser Himalaya
MBT
Bhramaputra River
Naga hills
Guwahati
Assam
Shillong
Mount Loimue
Jade Mines
Putao
Xuelong shan
Gaoligong Shan
Dali
Diancang Shan
Myitkyina
Bhamo
Taung Thonlong
MVK
Manipur
B' DESH
KGR
GS
TMB
MMB
Mogok
Wanding fault
Nanting fault
Ailao Shan
Red River fault
YANGTSE
Simao basin
Chindwin basin
WEST MYANMAR
Mizoram
Indo-Burma ranges
Ganges delta
Chittagong
Coxs Bazar
Kyanigan
Mandalay
Belin Kyaukse
SHAN-THAI
Lincang fault
Mt. Victoria
Mt. Popa
Minbu basin
Meiktila
Yebokson
Mengxing fault
Dien Ben Phu fault
Sagaing fault
Ramree Is.
Arakan-Yoma
Chiang Rai
Luang Prabang
Mai Sariang fault
Chiang Mai
Nan-Uttaradit suture
BAY OF BENGAL
Vientiane
Pathein basin
Langsang gneiss
Yangon
Moulmein
Mae Ping fault
Sukhotai-Lao fold belt
Irrawaddy delta
Three Pagodas fault
Andaman subduction zone
ANDAMAN SEA
Bangkok
Chonburi
Andaman Islands
Mergui
Gulf of Thailand
FIGUREs 1B, C
Gangdese batholith (105-c. 50Ma)
Yarlung Tsangpo suture zone
Mesozoic shelf margin sediments (+Upper Pz)
High Himalaya metamorphic rocks
Lesser Himalaya
Bhramaputra basin Tertiary molasse sediments
Shillong plateau PreCambrian
LHASA BLOCK
INDIAN PLATE
Quaternary calc-alkaline volcanoes
Naga-Chin-Arakan Yoma Ranges
Mt. Victoria-Kawlun belt
MVK
Jade Mines belt HP ophiolites
JM
Katha-Gangaw ranges
KGR
Tagaung-Myktyina belt
TMB
Mogok metamorphic belt
MMB
Chiang Mai-Lincang belt
Gaoligong-Salween gneisses
GS
Red River-Ailao Shan Metamorphic complexes
BURMA PLATE
90
92
94
96
98
100
30
28
26
24
22
20
18
16
14

Figure1A

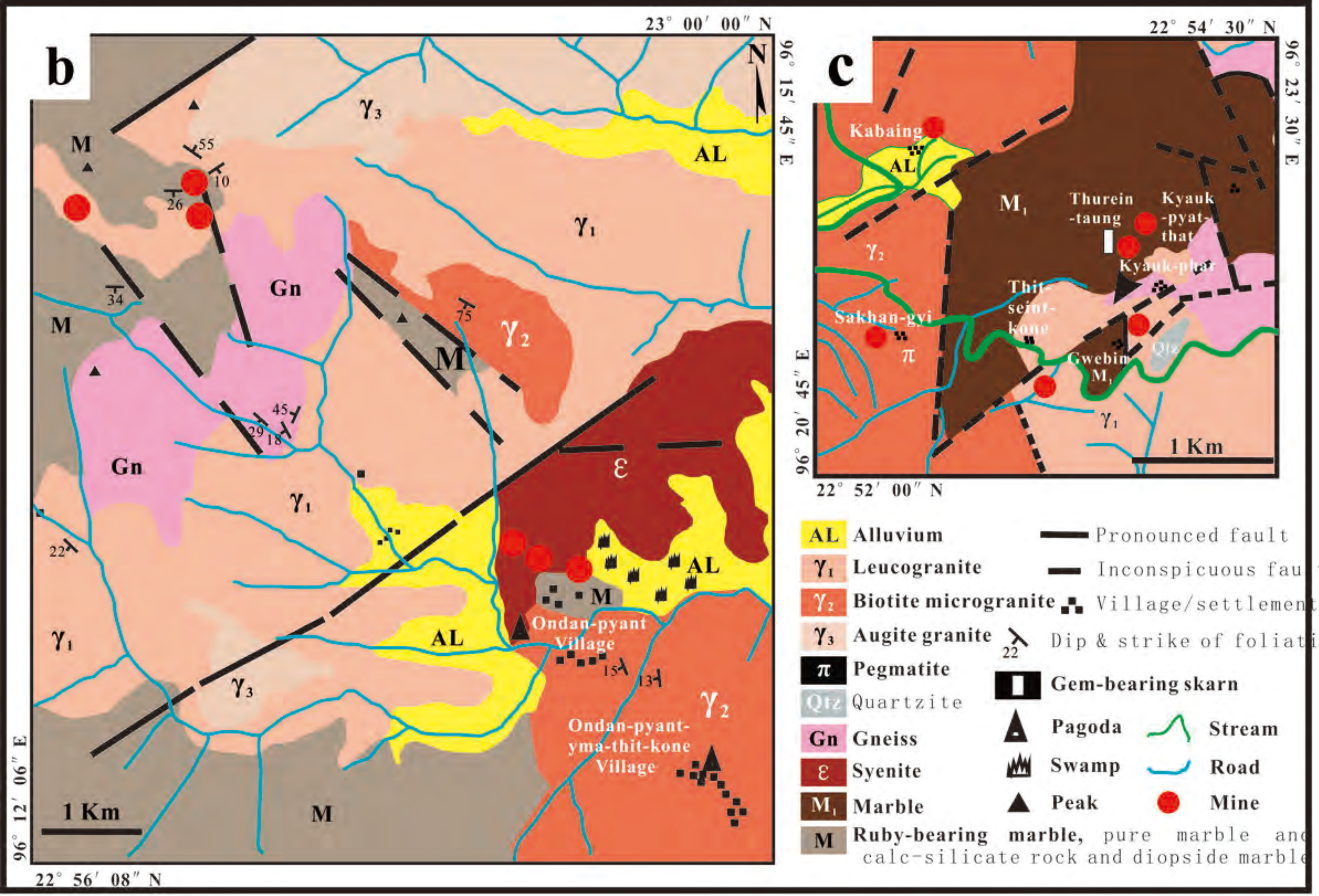
b
c
23° 00′ 00″ N
96° 15′ 45″ E
22° 56′ 08″ N
96° 12′ 06″ E
22° 54′ 30″ N
96° 23′ 30″ E
22° 52′ 00″ N
96° 20′ 45″ E
N
M
Gn
M
AL
γ1
γ2
γ3
ε
Ondan-pyant Village
Ondan-pyant-yma-thit-kone Village
1 Km
Kabaing
Thurein-taung
Kyauk-pyat-that
Kyauk-phar
Thit-seint-kone
Sakhan-gyi
Gwebin
M1
π
Qtz
AL Alluvium
γ1 Leucogranite
γ2 Biotite microgranite
γ3 Augite granite
π Pegmatite
Qtz Quartzite
Gn Gneiss
ε Syenite
M1 Marble
M Ruby-bearing marble, pure marble and calc-silicate rock and diopside marble
Pronounced fault
Inconspicuous fault
Village/settlement
Dip & strike of foliation
Gem-bearing skarn
Pagoda
Swamp
Peak
Stream
Road
Mine

Figures 1B, C

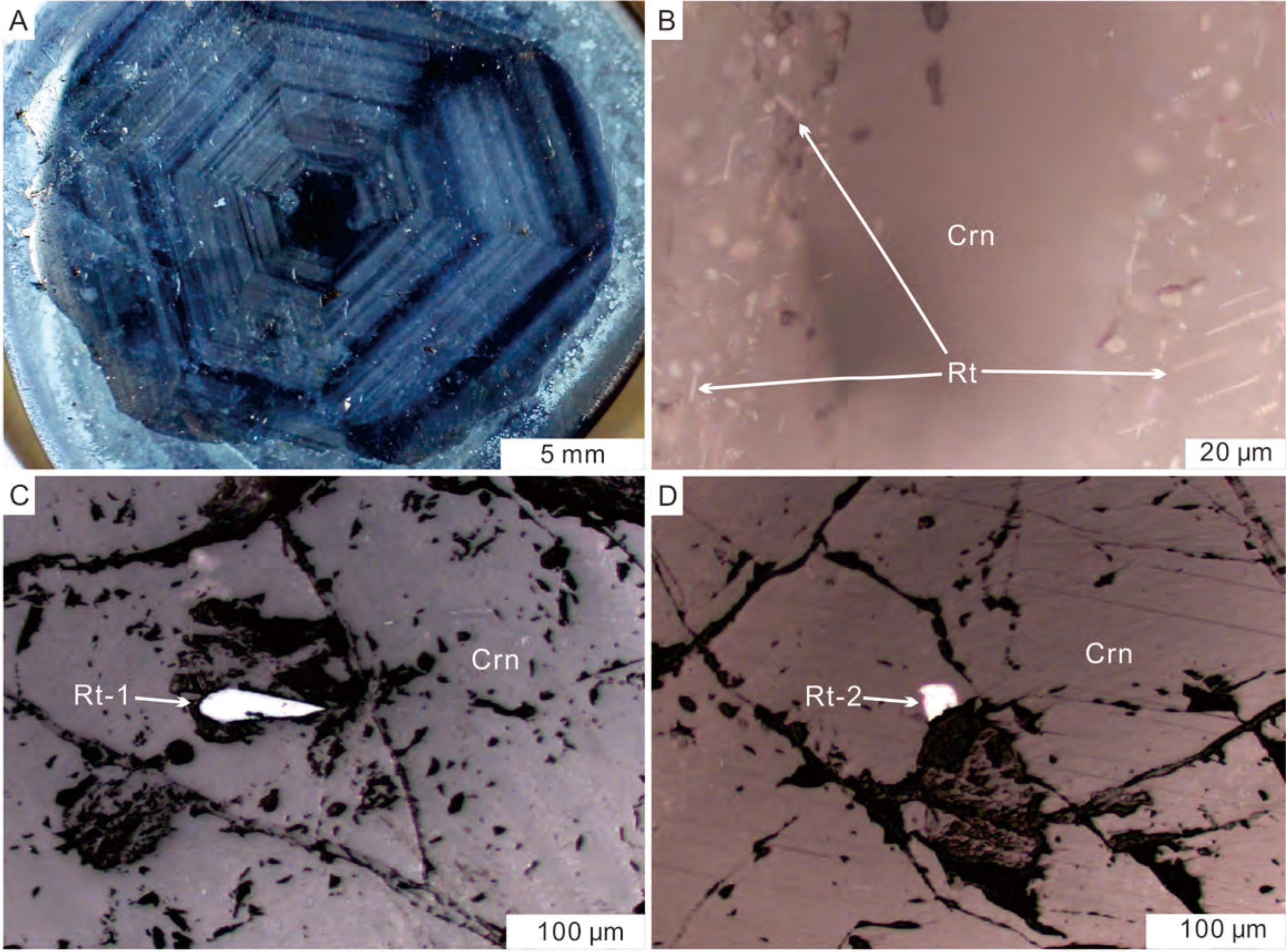

Figure 2

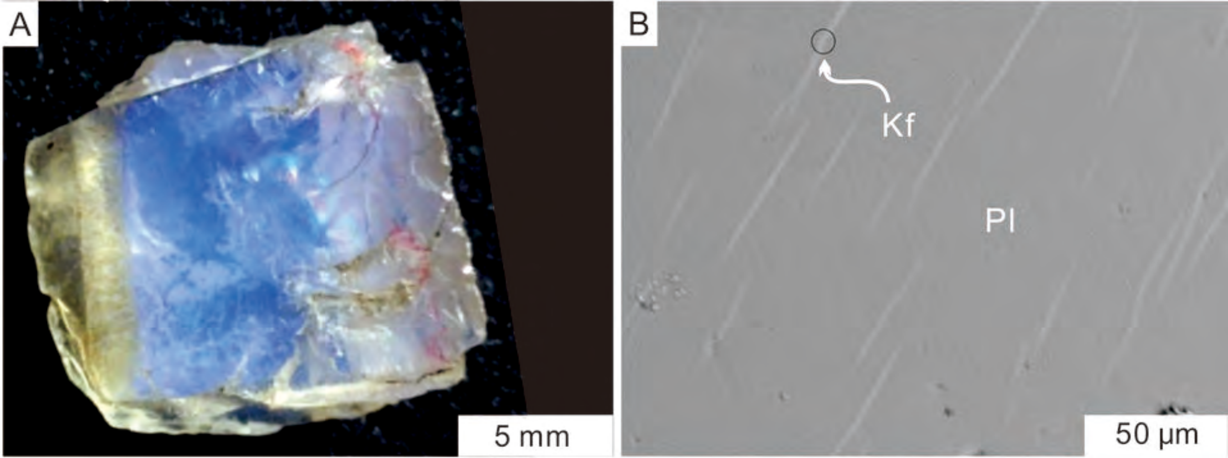

Figure 3

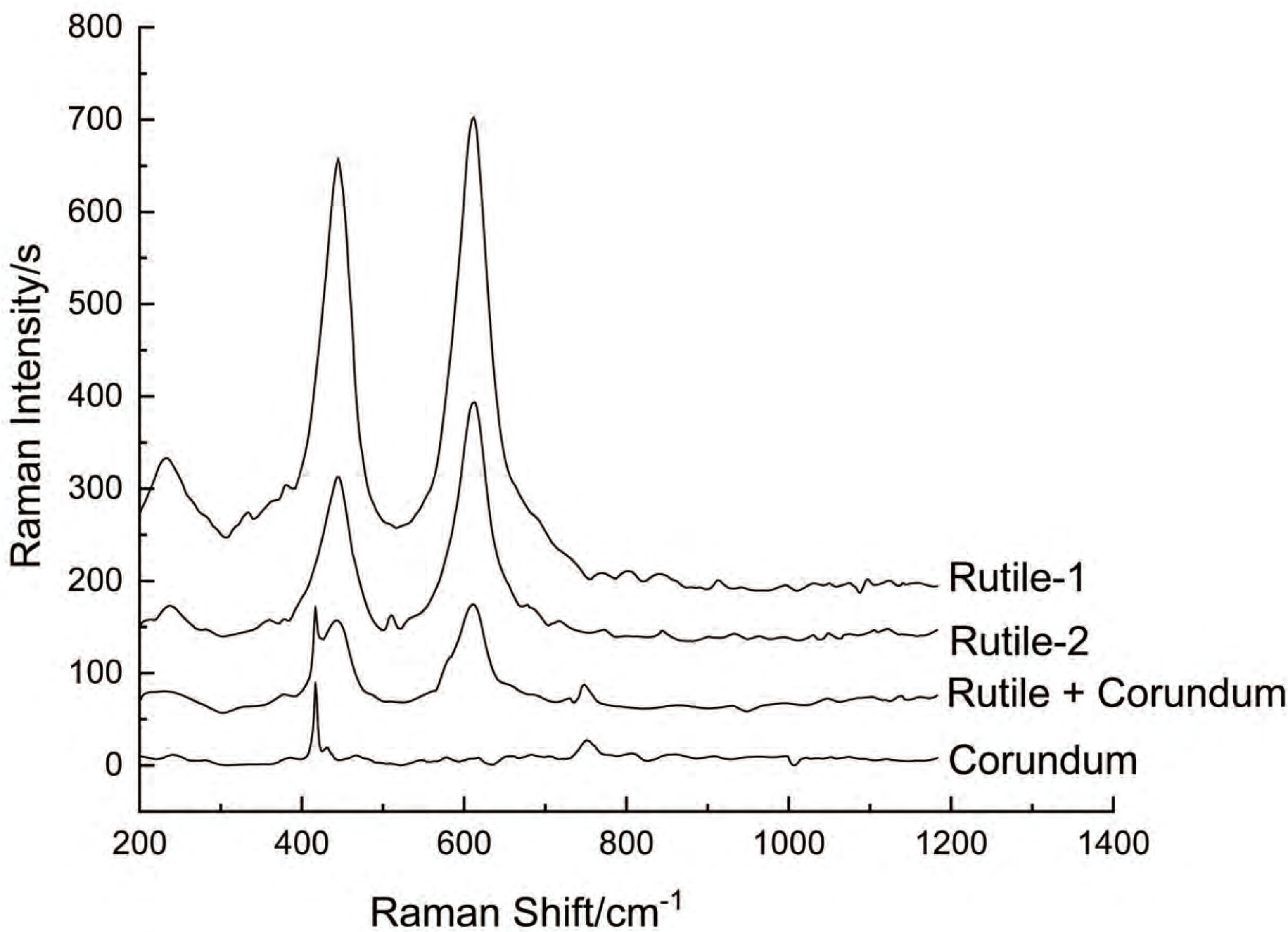
800
700
600
500
400
300
200
100
0
Raman Intensity/s
200
400
600
800
1000
1200
1400
Raman Shift/cm-1
Rutile-1
Rutile-2
Rutile + Corundum
Corundum

Figure 4

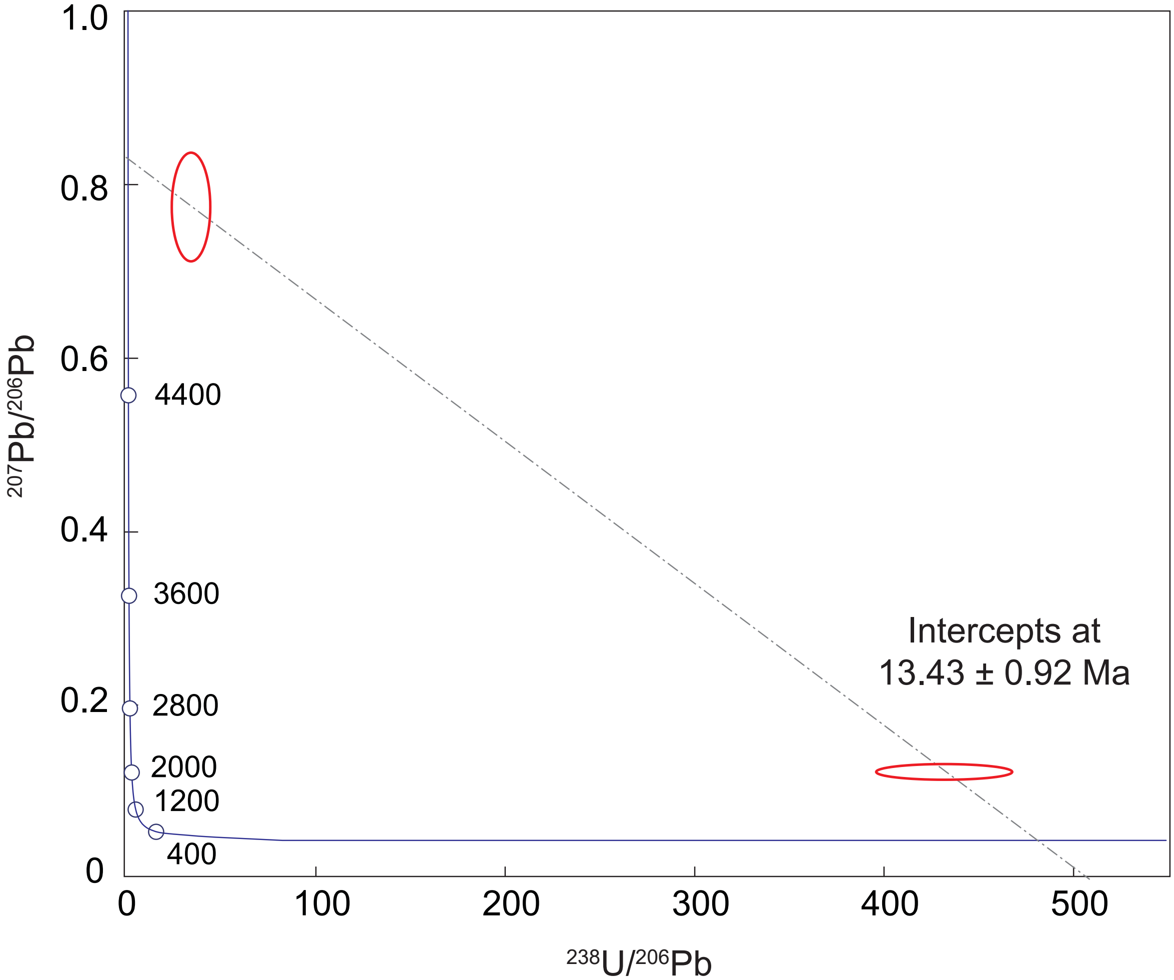
1.0
0.8
0.6
0.4
0.2
0
$^{207}Pb/^{206}Pb$
4400
3600
2800
2000
1200
400
Intercepts at
13.43 ± 0.92 Ma
0
100
200
300
400
500
$^{238}U/^{206}Pb$

Figure 5

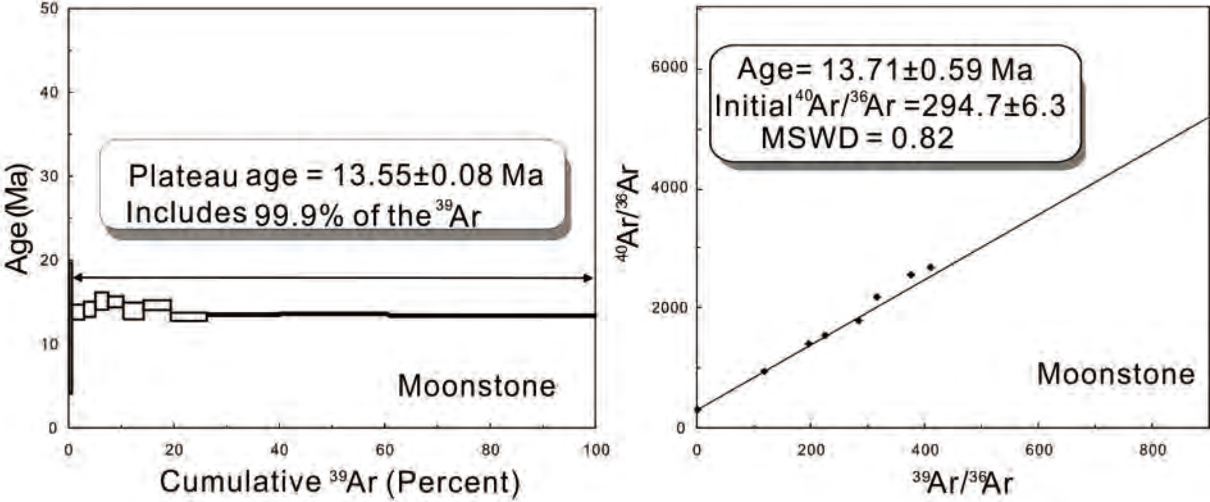
Plateau age = 13.55±0.08 Ma
Includes 99.9% of the 39Ar
Moonstone
Age (Ma)
Cumulative 39Ar (Percent)
Age= 13.71±0.59 Ma
Initial 40Ar/36Ar =294.7±6.3
MSWD = 0.82
Moonstone
40Ar/36Ar
39Ar/36Ar

Figure 6